Articles

Pronounced Effects of Ring Tilting on Rates of Intramolecular Electron Transfer in Polyalkyl-Substituted Mixed-Valence Biferrocenium Triiodides

Teng-Yuan Dong,*[,1] Shu-Hwei Lee,[1] Chung-Kay Chang,[1] Hsiu-Mei Lin,[1] and Kuan-Jiuh Lin[2]

Department of Chemistry, National Sun Yat-Sen University, Kaohsiung, Taiwan, and the Institute of Chemistry, Academia Sinica, Nankang, Taipei, Taiwan

Received December 6, 1996[⊗]

Relatively minor perturbations caused by Cp ring substituents in a series of mixed-valence biferrocenium cations have pronounced effects on the electronic structure and rate of intramolecular electron transfer. The X-ray structures of 1′,2′,1‴,2‴-tetrapropylbiferrocene, 1′,2′,1‴,2‴-tetrabenzylbiferrocene, 1′,3′,1‴,3‴-tetrapropylbiferrocene, 1′,3′,1‴,3‴-tetrabenzylbiferrocene, and their corresponding mixed-valence biferrocenium triiodide salts have been determined at 298 K. The rates of intramolecular electron transfer in the mixed-valence cations were estimated by variable-temperature ^{57}Fe Mössbauer spectroscopy (time scale $\sim 10^7$ s^{-1}). The features in all of the 80 K spectra include two doublets, one with a quadrupole splitting (ΔE_Q) of ~2 mm s^{-1} (Fe(II) site) and the other with ΔE_Q = ~0.6 mm s^{-1} (Fe(III) site). This pattern of two doublets is expected for a mixed-valence biferrocenium cation which is valence-trapped on the time scale of the Mössbauer experiment (electron-transfer rate < $\sim 10^7$ s^{-1} in the solid state). Increasing the sample temperature in 1′,2′,1‴,2‴-tetrapropylbiferrocenium triiodide, 1′,2′,1‴,2‴-tetrabenzylbiferrocenium triiodide, and 1′,3′,1‴,3‴-tetrabenzylbiferrocenium triiodide causes the two doublets to move together with no discernible line broadening, eventually becoming a single "average-valence" doublet at temperatures of 295, 265, and 190 K, respectively. In the case of 1′,3′,1‴,3‴-tetrapropylbiferrocenium triiodide, the two doublets at low temperatures do not coalesce into an average-valence doublet at 300 K (electron-transfer rate < ~10 s^{-1} at 300 K). Thus, the micromodification of the relative positions of the alkyl substituents and the nature of the alkyl substituents has a dramatic influence on the rate of intramolecular electron transfer. The deviations of the Cp rings from the parallel position correlate quite well with the Mössbauer critical temperature for electronic delocalization−localization in mixed-valence cations. Qualitatively, we suggest that the metal nonbonding orbitals ($d_{x^2-y^2}$, d_{xy}) start to interact with the ligand π orbitals as the Cp rings tilt from the parallel position. On the basis of the density functional calculations, a theoretical explanation of the influence of bending back the Cp rings on the electron-transfer rates is presented. The electrochemical measurements, IR data, and near-IR spectra for these mixed-valence biferrocenium cations are also presented.

Introduction

The rich chemistry of bridged mixed-valence dimers, especially those of ruthenium dimers[3] and biferrocenium cations,[4−23] has captured considerable attention. Studies on these mixed-valence compounds have concentrated on the extent of electron delocalization, the shape

[⊗] Abstract published in *Advance ACS Abstracts,* May 15, 1997.

(1) National Sun Yat-Sen University.

(2) Academia Sinica.

(3) For reviews, see: (a) Day, P. *Int. Rev. Phys. Chem.* **1981**, *1*, 149. (b) *Mixed-Valence Compounds, Theory and Applications in Chemistry, Physics, Geology and Biology*; Brown, D. B., Ed.; Reidel Publishing, Co.: Boston, MA, 1980. (c) Creutz, C. *Prog. Inorg. Chem.* **1983**, *30*, 1−73. (d) Richardson, D. E.; Taube, H. *Coord. Chem. Rev.* **1984**, *60*, 107.

(4) Hendrickson, D. N.; Oh, S. M.; Dong, T.-Y.; Moore, M. F. *Comm. Inorg. Chem.* **1985**, *4*, 329.

(5) Dong, T.-Y.; Cohn, M. J.; Hendrickson, D. N.; Pierpont, C. G. *J. Am. Chem. Soc.* **1985**, *107*, 4777.

(6) Cohn, M. J.; Dong, T.-Y.; Hendrickson, D. N.; Geib, S. J.; Rheingold, A. L. *J. Chem. Soc., Chem. Commun.* **1985**, 1095.

(7) Dong, T.-Y.; Hendrickson, D. N.; Iwai, K.; Cohn, M. J.; Rheingold, A. L.; Sano, H.; Motoyama, S. *J. Am. Chem. Soc.* **1985**, *107*, 7996.

(8) Iijima, S.; Saida, R.; Motoyama, I.; Sano, H. *Bull. Chem. Soc. Jpn.* **1981**, *54*, 1375.

(9) Nakashima, S.; Masuda, Y.; Motoyama, I.; Sano, H. *Bull. Chem. Soc. Jpn.* **1987**, *60*, 1673.

(10) Kai, M.; Katada, M.; Sano, H. *Chem. Lett.* **1988**, 1523.

(11) Dong, T.-Y.; Kambara, T.; Hendrickson, D. N. *J. Am. Chem. Soc.* **1986**, *108*, 5857.

(12) Dong, T.-Y.; Schei, C. C.; Hsu, T. L.; Lee, S. L.; Li, S. J. *Inorg. Chem.* **1991**, *30*, 2457.

(13) Webb, R. J.; Geib, S. J.; Staley, D. L.; Rheingold, A. L.; Hendrickson, D. N. *J. Am. Chem. Soc.* **1990**, *112*, 5031.

S0276-7333(96)01032-1 CCC: $14.00

Chart 1

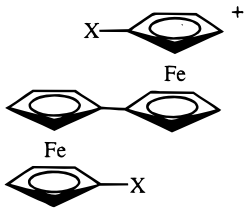

1 X = H **5** X = C_4H_9
2 X = CH_3 **6** X = I
3 X = C_2H_5 **7** X = Br
4 X = C_3H_7 **8** X = Cl

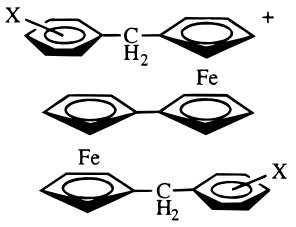

9 X = H n = 0
10 X = p-I n = 0
11 X = p-Br n = 1
12 X = p-Cl n = 0
13 X = o-I n = 0
14 X = o-Br n = 0

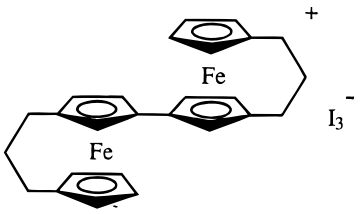

15

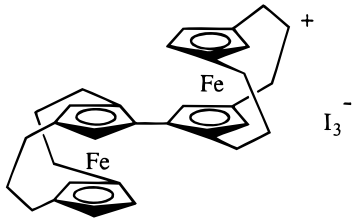

16

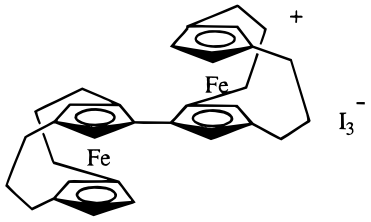

17

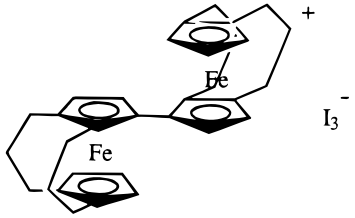

18

of the corresponding intervalence transfer (IT) band, and the role of the bridge in the electron-transfer process. Their physical properties have been discussed in light of Hush's model[24] and the PKS model.[25]

The series of mixed-valence biferrocenium triiodide salts (**1**−**14**, Chart 1), fulvalenide-bridged mixed-valence compounds, has been studied extensively in the solid state regarding the nature of the electronic structure in the ground state, various structural factors, and lattice dynamics,[6−10] including the electronic and vibronic coupling between two metal ions, the nature of the counterion,[11−14] and the cation−anion interactions.[26]

Compounds **3**−**5** and **9** give unusual temperature-dependent Mössbauer spectra.[4−8] At temperatures below 200 K, they show two doublets, one for the Fe^{II} and the other for the Fe^{III} sites. Increasing the sample temperature in each case causes the two doublets to move together with no discernible line broadening, eventually becoming a single "average-valence" doublet at temperatures of 275, 245, 275, and 260 K. The Mössbauer results indicate that compound **2** has a valence-trapped electronic structure (electron-transfer rate less than $\sim 10^7$ s^{-1} in solid state).[27] Hendrickson suggested[4] that there is an onset of dynamics associated with the counterions in the dialkylbiferrocenium cation,

(14) Webb, R. J.; Rheingold, A. L.; Geib, S. J.; Staley, D. L.; Hendrickson, D. N. *Angew. Chem., Int. Ed. Engl.* **1989**, *28*, 1388.
(15) Nakashima, S.; Katada, M.; Motoyama, I.; Sano, H. *Bull. Chem. Soc. Jpn.* **1987**, *60*, 2253.
(16) Dong, T.-Y.; Kambara, T.; Hendrickson, D. N. *J. Am. Chem. Soc.* **1986**, *108*, 4423.
(17) Sorai, M.; Nishimori, A.; Hendrickson, D. N.; Dong, T.-Y.; Cohn, M. J. *J. Am. Chem. Soc.* **1987**, *109*, 4266.
(18) Kambara, T.; Hendrickson, D. N.; Dong, T.-Y.; Cohn, M. J. *J. Chem. Phys.* **1987**, *86*, 2326.
(19) Konno, M.; Hyodo, S.; Iijima, S. *Bull. Chem. Soc. Jpn.* **1982**, *55*, 2327.
(20) Dong, T.-Y.; Hwang, M. Y.; Schei, C. C.; Peng, S. M.; Yeh, S. K. *J. Organomet. Chem.* **1989**, *369*, C33.
(21) Dong, T.-Y.; Schei, C. C.; Hwang, M. Y.; Lee, T. Y.; Yeh, S. K.; Wen, Y. S. *Organometallics* **1992**, *11*, 573.
(22) Dong, T.-Y.; Chou, C. Y. *J. Chem. Soc., Chem. Commun.* **1990**, 1332.
(23) Dong, T.-Y.; Lee, T. Y.; Lin, H. M. *J. Organomet. Chem.* **1992**, 427.
(24) Hush, N. S. *Prog. Inorg. Chem.* **1967**, *8*, 391.
(25) Wong, K. Y.; Schatz, P. N. *Prog. Inorg. Chem.* **1981**, *28*, 369 and references therein.
(26) Kambara, T.; Hendrickson, D. N.; Dong, T.-Y.; Cohn, M. J. *J. Chem. Phys.* **1987**, *86*, 2362.
(27) Nakashima, S.; Katada, M.; Motoyama, I.; Sano, H. *Bull. Chem. Soc. Jpn.* **1987**, *60*, 2253.

and this probably influences the rate of intramolecular electron transfer. Recently, we found[20,21] that the interactions between the cation and anion in **10**−**14** undoubtedly alter the potential energy surface of the mixed-valence molecule and, therefore, the rate of intramolecular electron transfer. Mixed-valence cations of **10** and **12** are localized on the time scale of the Mössbauer experiment. Furthermore, compound **11** has a valence-trapped electronic structure at temperatures below 150 K and becomes a valence-detrapped electronic structure at a temperature of ∼200 K. In comparison with para-substituted compounds (**10**−**12**), a valence-detrapped electronic structure is seen even at 77 K for ortho-substituted mixed-valence compounds of **13** and **14**. We suggested that relatively minor perturbations caused by interactions between neighboring cations and anions have pronounced effects on electron transfer.[22,28−30]

A recent interesting finding is that there is a significant influence on the electron-transfer rate in the mixed-valence biferrocenium salts (**15**−**18**) when the cyclopentadienyl (Cp) rings in each ferrocenyl moiety are tilted from a parallel relation between the two Cp rings around the Fe ion. Such a structural modification would lead to greater metal−ligand interactions as the rings tilt.

In our previous paper,[29] we also suggested that the difference in the electron-transfer rates for the series of dialkylbiferrocenium cations is mainly due to the degree of tilting of the Cp rings from the parallel geometry. We found that deviations of the Cp rings from the parallel position correlate quite well with the critical temperature of electronic delocalization−localization in mixed-valence biferrocenium salts. In this paper, we suggest that structural micromodifications in mixed-valence biferrocenium cations have certain important effects on the intramolecular electron-transfer rate. To study the influence of polyalkylbiferrocenium triiodide salts, we have prepared a series of polyalkylbiferrocenium triiodide salts.

Results and Discussion

Polyalkylbiferrocenium triiodide salts were prepared by coupling the corresponding bromoferrocenes, using activated Cu as a catalyst (Scheme 1). Mixed-valence compounds **26** and **27** were prepared by oxidizing the corresponding neutral biferrocenes with I_2. The resulting microcrystalline samples were recrystallized from a CH_2Cl_2/hexane solution. More crystalline samples, prepared by slowly diffusing hexane into a CH_2Cl_2 solution containing the corresponding biferrocenium triiodides, were used for all of the physical data measurements. Before the new physical data are described, a summary of the single-crystal X-ray structural results obtained for **24b**,**c**, **25b**,**c**, **26b**,**c**, and **27b**,**c** are presented first. X-ray crystallographic studies of these compounds were undertaken to elucidate the structures which are difficult to determine with certainty using NMR spectroscopy. It also helps in understanding the geometric influences of the Cp ring tilting on the rates of electron transfer in the series of mixed-valence biferrocenium cations.

Molecular Structures of 24−**27.** Details of the X-ray crystal data collections and unit-cell parameters of **24b**,**c**, **25b**,**c**, **26b**,**c**, and **27b**,**c** are given in Tables 1 and 2, and their molecular structures are shown in Figures 1−8. Selected bond distances and angles are given in Tables 3 and 4. These neutral and mixed-valence compounds exist in a trans conformation with the two iron ions on opposite sides of the planar fulvalenide bridge observed for most biferrocenes and biferrocenium cations. The two Cp rings in the fulvalenide bridge are crystallographically coplanar for these compounds. Thus, the π interaction between the two ferrocenyl units in each molecule is not destroyed. We believe that the degree of coplanarity between the two Cp rings in the fulvalenide bridge plays a most important role in determining the magnitude of the electron-transfer rate.

In the neutral complexes **24b**,**c** and **25b**,**c**, the average distance from the iron atom to the two Cp rings are 1.650(3), 1.645(5), 1.646(3), and 1.651(5) Å, respectively. Furthermore, there is no significant difference between the Fe−Cp distance and the Fe−fulvalenide distance. Inspection of these Fe−Cp distances shows that these values are closer to the value of 1.65 Å found for ferrocene[31] than to the value of 1.70 Å found for the ferrocenium ion.[32]

The respective dihedral angles between the two least-squares planes of the Cp rings for a given ferrocenyl moiety in **24b**,**c** and **25b**,**c** are 1.2(2), 0.7(2), 0.8(2), and 0.3(7)°, while the two Cp rings bonded to each iron ion are nearly eclipsed, with respective average staggering angles of 2.2(5), 6.5(5), 6.8(4), and 17.9(5)°. Each C−C bond length in the Cp ring agrees well with that in ferrocene (average value of 1.42 Å).[31] Mean bond distances from the Fe atom to the ring carbon atoms in **24b**,**c** and **25b**,**c** are 2.044(5), 2.043(4), 2.041(5), and 2.043(9) Å, respectively. These values agree well with the value of 2.045 Å observed for ferrocene.[31]

In the case of mixed-valence compounds **26b**,**c** and **27b**,**c**, the Fe−Cp distances are 1.671(6), 1.675(2), 1.672(1), and 1.668(8) Å, respectively. Each value is larger than that for the corresponding neutral compound. Furthermore, inspection of these Fe−Cp distances in mixed-valence cations shows that these values lie midway between the value of 1.65 Å found for ferrocene[31] and the value of 1.70 Å found for the ferrocenium ion.[32] The average Fe−C bond distances in **26b**,**c** and **27b**,**c** are 2.07(1), 2.068(4), 2.07(2), and 2.06(2) Å, respectively. The average Fe−C bond distance for a given mixed-valence cation is marginally larger than that in the corresponding neutral biferrocene.

Furthermore, the average Fe−C distances of these mixed-valence compounds are very similar, and the values also lie midway between the 2.045 Å distance observed for ferrocene[31] and the 2.075 Å distance observed for ferrocenium cations.[32] Such an increase in the Fe−C and Fe−Cp distances has been observed when ferrocenes are oxidized to the corresponding

(28) Dong, T.-Y.; Chang, C. K.; Huang, C. H.; Wen, Y. S.; Lee, S. L.; Chen, J. A.; Yeh, W. Y.; Yeh, A. *J. Chem. Soc., Chem. Commun.* **1992**, 526.
(29) Dong, T.-Y.; Huang, C. H.; Chang, C. K.; Wen, Y. S.; Lee, S. L.; Chen, J. A.; Yeh, W. Y.; Yeh, A. *J. Am. Chem. Soc.* **1993**, *115*, 6357.
(30) Dong, T.-Y.; Lee, S. H.; Chang, C. K.; Lin, K. J. *J. Chem. Soc., Chem. Commun.* **1995**, 2453.
(31) Seiler, P.; Dunitz, J. D. *Acta Crystallogr., Sect. B* **1979**, *35*, 1068.
(32) Mammano, N. J.; Zalkin, A.; Landers, A.; Rheingold, A. L. *Inorg. Chem.* **1977**, *16*, 297.
(33) Konno, M.; Sano, H. *Bull. Chem. Soc. Jpn.* **1988**, *61*, 1455.

Scheme 1

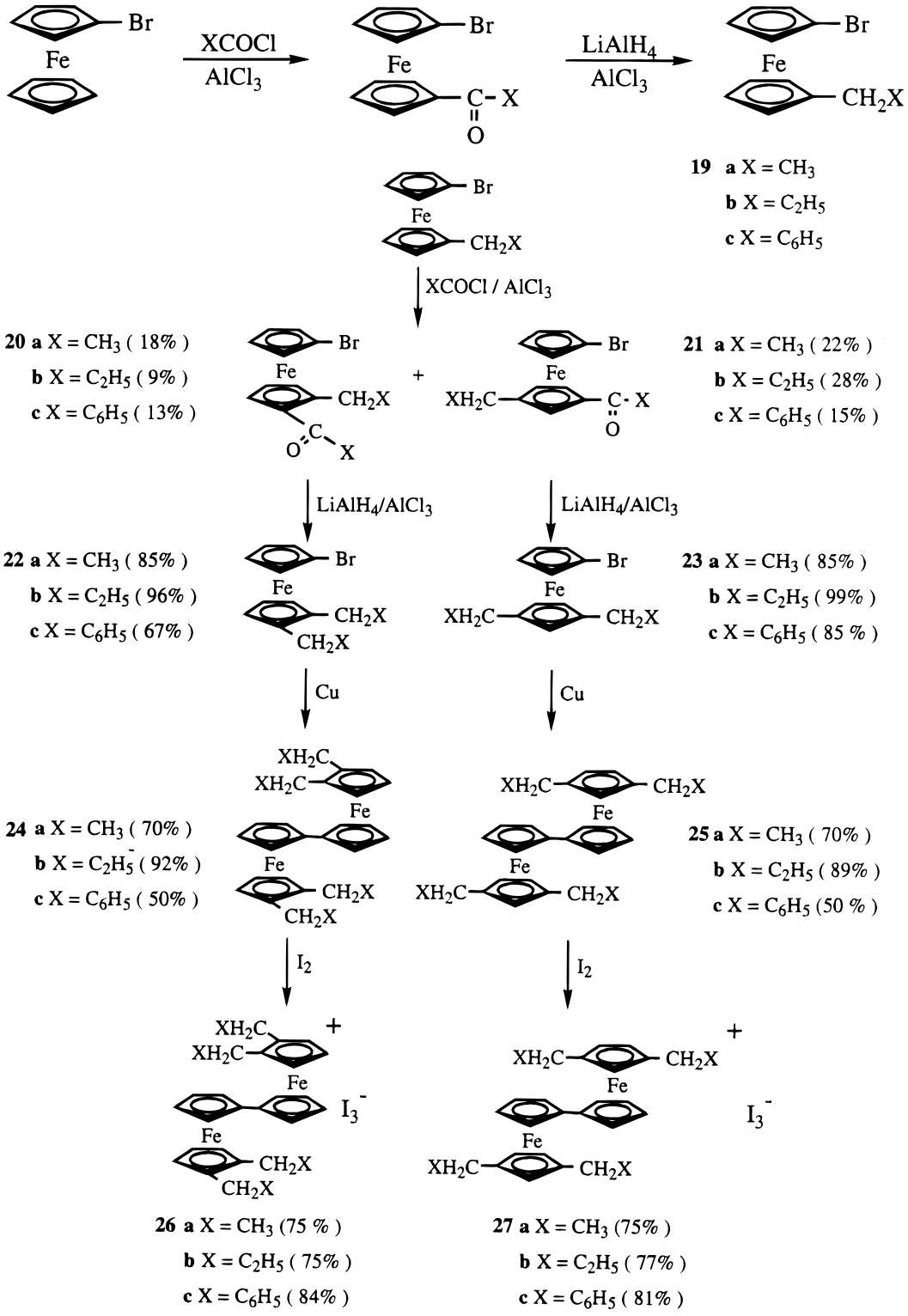

ferrocenium cations.[21,32] There is no significant difference for the average C−C bond distances in the Cp rings in these new mixed-valence compounds. The two Cp rings in each ferrocenyl moiety in **26b**,**c** and **27b**,**c** are also nearly eclipsed, with average staggering angles of 0.4(6), 5.9(2), 16.5(9), and 3.5(5) °, respectively.

In our previous papers,[28,29] we suggested that the degree of tilting of the Cp rings from the parallel geometry plays an important role in determining the rates of electron transfer in the series of mixed-valence biferrocenium triiodide salts. In this new series of mixed-valence compounds **26b**,**c** and **27b**,**c**, the least-squares planes of the Cp rings form dihedral angles of 3.9(5), 4.2(2), 4(1), and 6.6(7)°, respectively. A direct comparison of these important structural parameters between series of alkylbiferrocenium and polyalkylbiferrocenium triiodide salts is made (Table 5). From Table 5 and Figure 9, it can be easily seen that the decrease of the critical temperatures for the delocalization−localization transition (Mössbauer spectroscopy $\sim 10^7$ s^{-1}) in the series of mixed-valence biferrocenium salts is accompanied by the increase of the tilting angle.

Table 1. Experimental and Crystal Data for the X-ray Structures of Neutral Biferrocenes

	24b	**24c**	**25b**	**25c**
formula	$C_{32}H_{42}Fe_2$	$C_{48}H_{42}Fe_2$	$C_{32}H_{42}Fe_2$	$C_{48}H_{42}Fe_2$
mw	538.37	730.55	538.38	730.55
cryst syst	triclinic	monoclinic	triclinic	monoclinic
space group	$P\bar{1}$	$P2_1/c$	$P\bar{1}$	$P2_1/n$
a, Å	8.175(1)	12.694(5)	7.628(3)	13.342(3)
b, Å	9.373(2)	17.300(6)	10.046(3)	6.0182(8)
c, Å	10.381(2)	8.135(3)	10.238(3)	22.185(4)
α, deg	73.07(1)		64.80(2)	
β, deg	88.90(1)	91.29(4)	76.20(3)	100.18(1)
γ, deg	65.71(1)		75.97(3)	
ρ_{calcd}, g cm^{-3}	1.298	1.36	1.314	1.384
V, Å^3	688.96(2)	1786(1)	680.5(4)	1753.2(5)
Z	1	2	1	2
μ, mm^{-1}	1.07	0.845	8.88	1.72
λ, Å	0.710 69	0.710 69	0.710 69	0.710 69
2θ limits, deg	44.9	50.0	44.9	45.0
max, min trans coeff	0.9991, 0.9322	1.0000, 0.8825	0.9998, 0.8611	0.9942, 0.8760
R_f	0.037	0.041	0.044	0.044
R_{wf}	0.038	0.050	0.051	0.043

Table 2. Experimental and Crystal Data for the X-ray Structures of Mixed-Valence Biferrocenium Triiodides

	26b	**26c**	**27b**	**27c**
formula	$C_{32}H_{42}Fe_2I_3$	$C_{48}H_{42}Fe_2I_3$	$C_{32}H_{42}Fe_2I_3$	$C_{48}H_{42}Fe_2I_3$
mw	919.08	1111.26	919.08	1111.26
cryst syst	triclinic	triclinic	monoclinic	triclinic
space group	$P\bar{1}$	$P\bar{1}$	$P2_1/n$	$P\bar{1}$
a, Å	8.764(1)	9.307(2)	13.647(4)	9.517(3)
b, Å	9.329(3)	10.626(2)	10.171(2)	10.688(3)
c, Å	11.240(3)	10.965(1)	13.929(4)	10.830(4)
α, deg	103.08(3)	76.82(1)		74.03(3)
β, deg	97.88(1)	85.59(1)	116.39(2)	79.81(3)
γ, deg	102.80(2)	86.29(2)		89.53(3)
ρ_{calcd}, g cm^{-3}	1.783	1.755	1.762	1.772
V, Å^3	855.8(4)	1051.5(3)	1732.0(9)	1041.4(6)
Z	1	1	2	1
μ, mm^{-1}	7.09	5.79	6.97	6.32
λ, Å	0.710 69	0.710 69	0.710 69	0.710 69
2θ limits, deg	44.9	45.0	45.0	44.9
max, min trans coeff	0.9928, 0.8276	0.9978, 0.7107	0.9992, 0.5100	0.6294, 0.6266
R_f	0.038	0.034	0.067	0.057
R_{wf}	0.045	0.040	0.087	0.069

In other words, there is a correlation between the tilt angle and the rate of electron transfer. A detailed discussion based on density functional theoretical calculations is presented in the later sections.

The I_3^- anion is at the inversion center, showing a symmetric structure. The I−I bond distances in the series of new mixed-valence compounds are in accord with the accepted value of 2.92 Å reported for the free I_3^- ion.[34] The cations in this series of mixed-valence compounds are also at the inversion centers. The site symmetry imposed on each mixed-valence cation obviously requires that both iron ions of the cation are in equivalent positions, and this is consistent with our Mössbauer studies for the series of mixed-valence compounds.

In addition to the influence of the tilting of the Cp rings on the electron-transfer rate, we believe that the positioning of the triiodide anion relative to the mixed-valence cation also plays an important role in controlling

(34) Runsink, J.; Swen-Walstra, S.; Migchelsen, T. *Acta Crystallogr., Sect. B* **1972**, *28*, 1331.

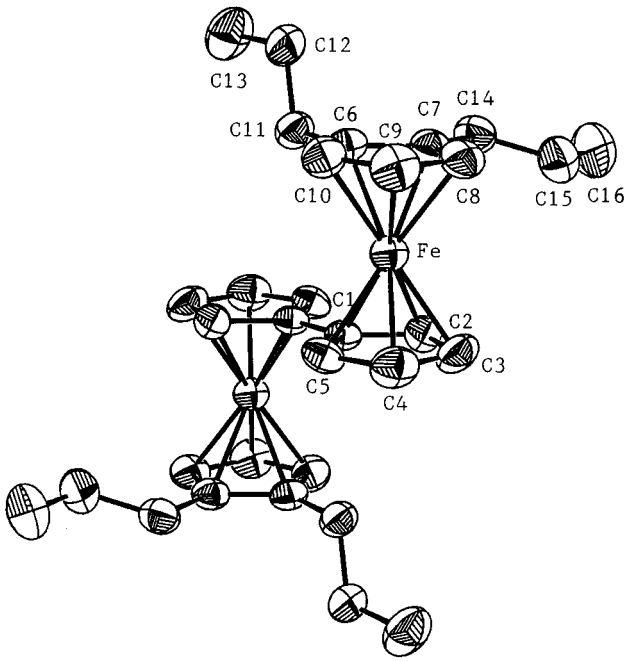

Figure 1. ORTEP drawing for **24b**, with 30% thermal ellipsoids.

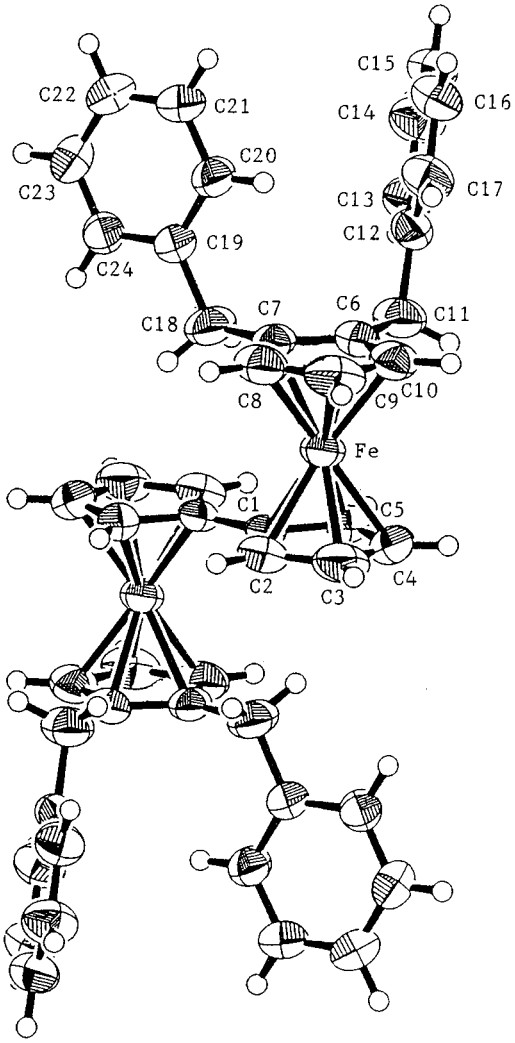

Figure 2. ORTEP drawing for **24c**, with 30% thermal ellipsoids.

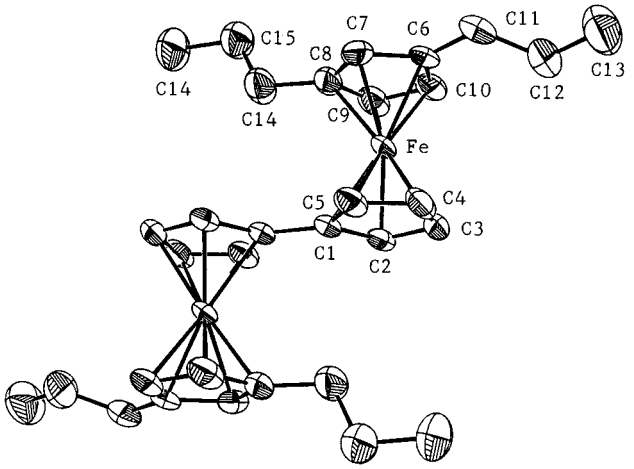

Figure 3. ORTEP drawing for **25b**, with 30% thermal ellipsoids.

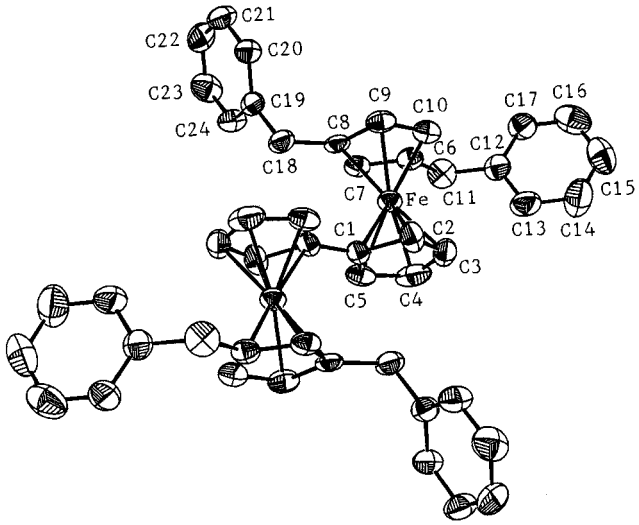

Figure 4. ORTEP drawing for **25c**, with 30% thermal ellipsoids.

the rate of electron transfer. The triiodide moiety in these polyalkyl-substituted mixed-valence biferrocenium compounds is relatively perpendicular to the fulvalenide ligand as, found in **1**,[7] **3**−**6**,[11,19,33] and **27a**.[29] With such a similar cation−anion relationship, we can potentially discover the influence of the tilting of the Cp rings on the rate of electron-transfer.

Electrochemical Measurements. Electrochemical data for the neutral compounds (**24b**,**c** and **25b**,**c**), as well as those for some other relevant compounds, are shown in Table 6. These binuclear biferrocenes all undergo two successive reversible one-electron oxidations to yield the mono- and then the dication. Electrochemical reversibility is demonstrated by the peak-to-peak separation between the resolved reduction and oxidation wave maxima (Table 6) and a 1:1 relationship of the cathodic and anodic peak currents (I_c/I_a Table 6).

The effect of the alkyl substituents on the stability of the Fe(III) state is illustrated by the shift of the half-wave potential. In general, electron-donating groups stabilize the ferrocenium cation, lowering the half-wave potential, while electron-withdrawing groups have the opposite effect. Comparison of the half-wave potentials of **24** and **25** with those of biferrocene and 1′,1‴-dialkylbiferrocenes indicates that the alkyl substituent clearly acts as a net electron donor. Furthermore, it is important to find that the first or second half-wave potential of **24b** is very similar with that of **25b**. The same observation also occurs between **24c** and **25c**. In other words, changing the positions of the alkyl substituents from ortho to meta does not instantaneously change the half-wave potential. It seems that the electronic effect of the alkyl substituent has nothing to do with the position of substitution.

It has been demonstrated that the magnitude of the peak-to-peak separation ($\Delta E_{1/2}$) gives an indication of the interaction between two Fe sites.[35] Making a comparison of the magnitude of $\Delta E_{1/2}$ for various polyalkyl-substituted biferrocenes indicates that the magnitude of interaction between the two Fe sites is similar in solution. Thus, the interaction between the two Fe sites is insensitive to both the position of substitution and the nature of the substituent.

In eq 1, the abbreviations [3, 3], [2, 3], and [2, 2] denote the dioxidized salt, the monooxidized salt, and the neutral compound, respectively. From the value of $\Delta E_{1/2}$, the disproportionation equilibrium constant K (as shown in Table 6) can be calculated. In the studies of

$$[2,2] + [3,3] \overset{K}{\rightleftharpoons} 2[2,3] \qquad (1)$$

the intervalence transition band in the near-IR region, quantitative calculations based on the concentration of [2, 3] have been corrected for this equilibrium.

Electron Transfer in the Solid State. The rates of intramolecular electron transfer in the mixed-valence cations **26b**,**c** and **27b**,**c** were estimated by variable-temperature ^{57}Fe Mössbauer spectroscopy (time scale $\sim 10^7$ s^{-1}). The variable-temperature ^{57}Fe Mössbauer spectra of these compounds are shown in Figures 10−13. The various absorption peaks were fitted to Lorentzian lines. The resulting fitting parameters are collected in Table 7.

The features in all of the 80 K spectra include two doublets, one with a quadrupole splitting (ΔE_Q) of ∼2 mm s^{-1} (Fe(II) site) and the other with $\Delta E_Q = \sim 0.6$ mm s^{-1} (Fe(III) site). Both doublets have the same area, as deduced by a least-squares fitting. This pattern of two doublets is expected for a mixed-valence biferrocenium cation which is valence-trapped on the time scale of the Mössbauer experiment (electron-transfer rate < $\sim 10^7$ s^{-1} in the solid state). Increasing the sample temperature in **26b**,**c** and **27c** causes the two doublets to move together with no discernible line broadening, eventually becoming a single average-valence doublet at temperatures of 295, 265, and 190 K, respectively. In the case of **27b**, the two doublets at low temperatures do not coalesce into an average-valence doublet at 300 K (electron-transfer rate < $\sim 10^7$ s^{-1} at 300 K). Thus, the micromodification of the relative positions of alkyl substituents and the nature of alkyl substituents has a dramatic influence on the rate of intramolecular electron transfer. The ordering of intramolecular electron-transfer rates is **27c** > **26c** > **26b** > **27b**.

(35) (a) Morrison, W. H., Jr.; Krogsrud, S.; Hendrickson, D. N. *Inorg. Chem.* **1973**, *12*, 1998. (b) Bunel, E. E.; Campos, P.; Ruz, J.; Valle, L.; Chadwick, I.; Ana, M. S.; Gonzalez, G.; Manriquez, J. M. *Organometallics* **1988**, *7*, 474. (c) Atzkern, H.; Huber, B.; Köhler, F. H.; Müller, G.; Müller, R. *Organometallics* **1991**, *10*, 238. (d) Chukwu, R.; Hunter, A. D.; Santarsiero, B. D.; Bott, S. G.; Atwood, J. L.; Chassaignac, J. *Organometallics* **1992**, *11*, 589.

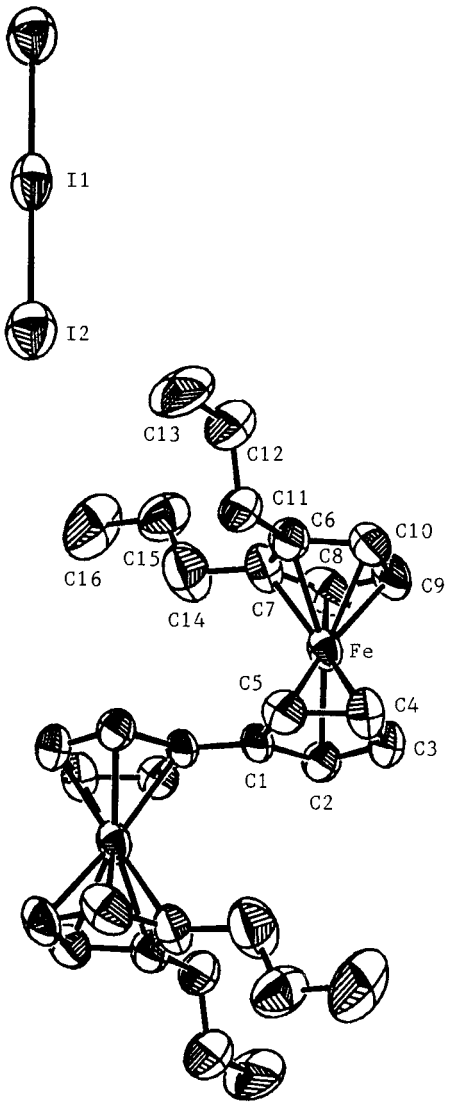

Figure 5. ORTEP drawing for **26b**, with 30% thermal ellipsoids.

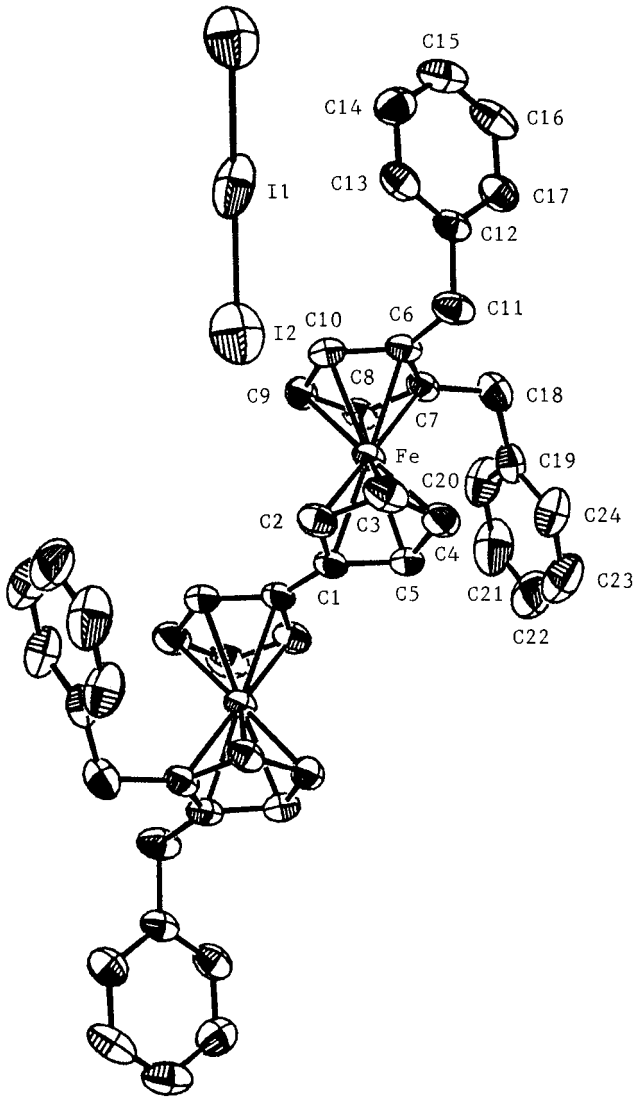

Figure 6. ORTEP drawing for **26c**, with 30% thermal ellipsoids.

We believe that the difference of the electron-transfer rates in the series of biferrocenium cations is not a result of the difference in the electronic effect of the alkyl substituents. The Mössbauer transition temperature of 1′,1‴-dipropylbiferrocenium triiodide (**4**) is 245 K. On the other hand, the Mössbauer T_c of **26b** and **27b** is 295 and >300 K, respectively. Similarly, the Mössbauer T_c of **26c** (265 K) is also higher than that of 1′,1‴-dibenzylbiferrocenium triiodide (260 K). Hence, an extra alkyl substituent on the Cp ring in **26b**,**c** and **27b** does not increase the rate of electron transfer. It is clear that the electronic effect of the alkyl is not additive by comparing the Mössbauer T_c. Further evidence can be gleaned from the peak-to-peak separation ($\Delta E_{1/2}$) mentioned in the section discussing the electrochemical measurements. In our previous papers, we found[29] that the deviations of the Cp rings from the parallel position correlate quite well with the Mössbauer critical temperature for electronic delocalization−localization in mixed-valence cations of **1**, **3**, **6**, and **27a**. As shown in Figure 9, the new series of mixed-valence compounds **26b**,**c** and **27c** also fit into the correlation of the tilt angle with the electron-transfer rate. Qualitatively, we suggested that the metal nonbonding orbitals ($d_{x^2-y^2}$, d_{xy}) start to interact with the ligand π orbitals as the Cp rings tilt from the parallel position.

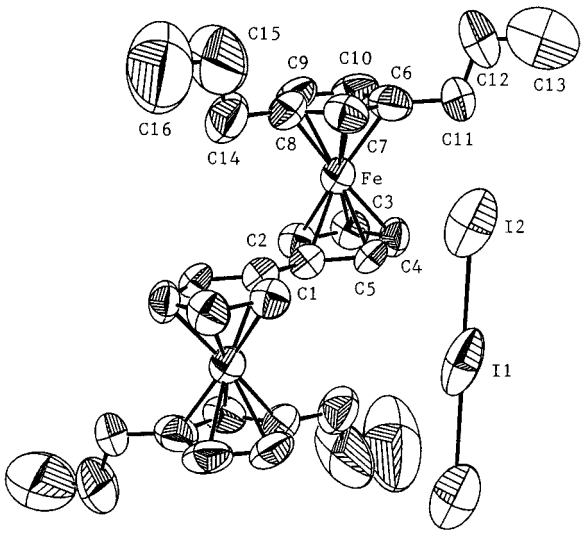

Figure 7. ORTEP drawing for **27b**, with 30% thermal ellipsoids.

The IR spectra of mixed-valence compounds **26b**,**c** and **27b**,**c** exhibit two C−H perpendicular bending

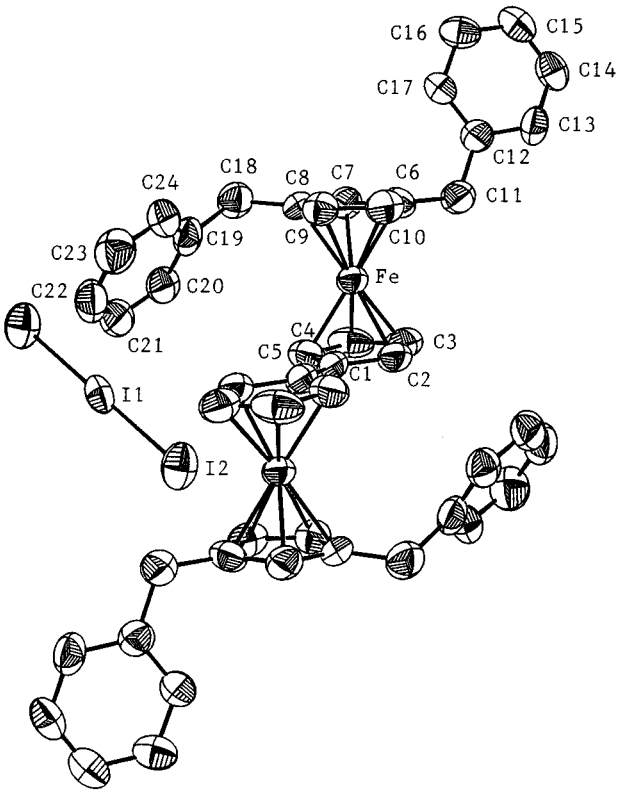

Figure 8. ORTEP drawing for **27c**, with 30% thermal ellipsoids.

bands, which may be readily assigned to Fe^{II} (~815 cm^{-1}) and Fe^{III} (~845 cm^{-1}) moieties. It is clear that compounds **26b**,**c** and **27b**,**c** are all localized on the IR time scale.

Electron Transfer in the Solution State. In common with most mixed-valence compounds, the mixed-valence compounds **26b**,**c** and **27b**,**c** in CH_2Cl_2 have an IT band at 4651 cm^{-1}, which is not present in the corresponding neutral compound or dioxidized ion. A description of the width of the IT band, the extent of electron delocalization, and the electron-transfer properties of the mixed-valence dimers has been given by Hush.[24] Hush has derived an expression for the bandwidth (in cm^{-1}) at half-maximum of the IT band of a localized homonuclear mixed-valence dimer at 300 K as

$$\Delta\nu_{1/2} = (2310\ \nu_{max})^{1/2} \qquad (2)$$

where ν_{max} is the frequency in cm^{-1} of the absorption maximum. For a system with harmonic nuclear motion, the energy of activation ΔE^* is related to the energy of the IT band maximum (ν_{max}) by the expression:

$$\Delta E^* = {}^1/_4\nu_{max} \qquad (3)$$

Furthermore, the magnitude of the delocalization can be obtained by a calculation of the delocalization parameter α^2 and electronic coupling H_{ab} from eqs 4 and 5. In eqs 4 and 5, ϵ_{max} is the extinction coefficient and

$$\alpha^2 = \{(4.24 \times 10^{-4})\epsilon_{max}(\Delta\nu_{1/2})\}/\{\nu_{max}d^2\} \qquad (4)$$

$$H_{ab} = \nu_{max}\alpha \qquad (5)$$

d (5.1 Å) is the donor−acceptor distance.[7] The rate constant (K_{et}) can be estimated from eq 6, where ν_{et} is the hopping frequency. The absorption maximum and

$$K_{et} = \nu_{et}\exp(-\nu_{max}/4K_BT) \qquad (6)$$

$$\nu_{et} = (2\pi/\hbar)H_{ab}{}^2(\pi/K_BT\nu_{max})^{1/2}$$

activation parameters calculated from eqs 2−6 were collected in Table 8, together with those for other relevant compounds.

The experimental α^2 value is the average of α^2 values for the ground and excited states. If delocalization is small, the electronic wave functions used for the overlap are relatively unperturbed. Thus, α^2 is a direct measure of the delocalization in the ground state. As shown in Table 8, there is good evidence for localized valences in **26b**,**c** and **27b**,**c**.

Influence of Ring Tilting on Solid-State Electron Transfer. The goal of this section is to present an explanation for the differences of electron-transfer rates in the series of mixed-valence cations.

In the past few years, we have made considerable progress in understanding what factors control the rate of intramolecular electron transfer in the solid state for mixed-valence biferrocenium salts. We found that the factors that are potentially important in controlling the rate of intramolecular electron transfer in a mixed-valence biferrocenium cation include the zero-point energy difference in the cation,[12] the nature of the counterion,[11−14] and the intermolecular cation−anion interactions.[18] In fact, the most important factor in

Table 3. Selected Bond Distances (Å) and Bond Angles (deg) for 24b,c and 26b,c

	24b	26b	24c	26c
		Distances		
Fe−C(1)	2.052(4)	2.09(1)	2.063(3)	2.110(4)
Fe−C(2)	2.037(5)	2.07(1)	2.039(3)	2.057(4)
Fe−C(3)	2.044(5)	2.05(1)	2.029(4)	2.049(4)
Fe−C(4)	2.043(5)	2.05(1)	2.039(4)	2.051(4)
Fe−C(5)	2.045(5)	2.054(1)	2.054(4)	2.063(4)
Fe−C(6)	2.054(5)	2.09(1)	2.036(3)	2.088(4)
Fe−C(7)	2.046(5)	2.10(1)	2.045(3)	2.096(4)
Fe−C(8)	2.036(5)	2.06(1)	2.042(4)	2.051(4)
Fe−C(9)	2.033(5)	2.05(1)	2.046(4)	2.052(4)
Fe−C(10)	2.048(5)	2.06(1)	2.040(4)	2.063(4)
C(1)−C(1)[a]	1.470(8)	1.43(2)	1.472(6)	1.438(7)
C(1)−C(2)	1.408(7)	1.45(1)	1.419(5)	1.438(6)
C(1)−C(5)	1.429(6)	1.43(2)	1.422(4)	1.435(6)
C(2)−C(3)	1.424(7)	1.43(2)	1.404(6)	1.420(6)
C(3)−C(4)	1.412(9)	1.41(2)	1.378(6)	1.406(7)
C(4)−C(5)	1.414(7)	1.42(2)	1.429(6)	1.423(6)
C(6)−C(7)	1.425(7)	1.44(2)	1.407(4)	1.434(6)
C(6)−C(10)	1.421(7)	1.44(2)	1.421(5)	1.429(6)
C(7)−C(8)	1.426(7)	1.42(2)	1.434(5)	1.421(5)
C(8)−C(9)	1.417(8)	1.43(2)	1.399(6)	1.416(6)
C(9)−C(10)	1.417(8)	1.43(2)	1.398(6)	1.423(5)
I(1)−I(2)		2.912(2)		2.536(4)
		Angles		
C(2)−C(1)−C(5)	107.2(4)	107.6(9)	107.2(3)	105.9(3)
C(1)−C(2)−C(3)	108.5(4)	106.3(9)	108.5(4)	108.9(4)
C(2)−C(3)−C(4)	108.0(4)	109.7(9)	108.5(4)	108.1(4)
C(3)−C(4)−C(5)	107.8(4)	108(1)	109.0(4)	108.3(4)
C(1)−C(5)−C(4)	108.4(4)	108.7(9)	106.9(4)	108.7(4)
C(7)−C(6)−C(10)	107.6(4)	107.3(9)	108.2(3)	107.5(3)
C(6)−C(7)−C(8)	107.3(4)	108(1)	106.6(3)	107.5(3)
C(7)−C(8)−C(9)	108.9(4)	109(1)	108.8(4)	109.0(3)
C(8)−C(9)−C(10)	107.1(4)	107.7(9)	107.8(3)	107.6(3)
C(6)−C(10)−C(9)	109.0(5)	108.3(1)	108.5(4)	108.4(3)
I(2)−I(1)−I(2)[b]		180.0		180.0

[a] Symmetry equivalents: $1-x, 1-y, 1-z$ for **24b**; $1-x, 1-y, 2-z$ for **26b**; and $1-x, 1-y, 2-z$ for **26c**. [b] Symmetry equivalents: $-x, -y, -z$ for **26b** and **26c**.

Table 4. Selected Bond Distances (Å) and Bond Angles (deg) for 25b,c and 27b,c

	25b	27b	25c	27c
		Distances		
Fe−C(1)	2.060(4)	2.10(2)	2.062(8)	2.10(1)
Fe−C(2)	2.036(5)	2.07(2)	2.056(9)	2.06(1)
Fe−C(3)	2.035(5)	2.06(2)	2.028(9)	2.02(2)
Fe−C(4)	2.038(5)	2.04(2)	2.04(1)	2.03(2)
Fe−C(5)	2.045(5)	2.06(1)	2.04(1)	2.07(1)
Fe−C(6)	2.047(4)	2.06(2)	2.055(8)	2.05(1)
Fe−C(7)	2.037(5)	2.06(2)	2.025(8)	2.06(1)
Fe−C(8)	2.044(5)	2.07(2)	2.052(8)	2.08(1)
Fe−C(9)	2.032(5)	2.09(2)	2.036(9)	2.06(1)
Fe−C(10)	2.040(5)	2.06(2)	2.04(1)	2.04(1)
C(1)−C(1)[a]	1.462(8)	1.42(3)	1.48(2)	1.43(3)
C(1)−C(2)	1.427(7)	1.46(2)	1.43(2)	1.42(2)
C(1)−C(5)	1.429(7)	1.46(2)	1.40(2)	1.43(2)
C(2)−C(3)	1.422(7)	1.42(3)	1.41(2)	1.38(3)
C(3)−C(4)	1.395(9)	1.42(3)	1.40(2)	1.40(3)
C(4)−C(5)	1.422(7)	1.41(3)	1.42(2)	1.41(2)
C(6)−C(7)	1.436(7)	1.46(3)	1.41(1)	1.40(2)
C(6)−C(10)	1.417(7)	1.44(3)	1.41(2)	1.43(2)
C(7)−C(8)	1.409(8)	1.44(3)	1.41(1)	1.44(2)
C(8)−C(9)	1.408(8)	1.40(3)	1.43(2)	1.39(2)
C(9)−C(10)	1.424(7)	1.39(3)	1.42(1)	1.42(2)
I(1)−I(2)		2.900(2)		2.920(2)
		Angles		
C(2)−C(1)−C(5)	107.4(4)	108(1)	107.8(8)	107(1)
C(1)−C(2)−C(3)	107.7(4)	107(2)	107(1)	108(2)
C(2)−C(3)−C(4)	108.8(4)	109(2)	110(1)	108(1)
C(3)−C(4)−C(5)	108.4(4)	110(2)	107(1)	109(2)
C(1)−C(5)−C(4)	107.8(4)	107(2)	109(1)	107(1)
C(7)−C(6)−C(10)	106.1(4)	104(2)	107.2(8)	108(1)
C(6)−C(7)−C(8)	109.4(4)	108(2)	110.5(9)	107(1)
C(7)−C(8)−C(9)	107.4(4)	108(2)	105.8(8)	109(1)
C(8)−C(9)−C(10)	108.4(5)	108(2)	108.7(8)	108(1)
C(6)−C(10)−C(9)	108.7(4)	112(2)	107.7(9)	108(1)
I(2)−I(1)−I(2)[b]		179.9		180.0

[a] Symmetry equivalents: $1-x$, $1-y$, $-z$ for **25b**, **27b**, **25c**, and **27c**. [b] Symmetry equivalents: $1-x$, $-y$, $-z$ for **27b**; $-x$, $-y$, $-z$ for **27c**.

Table 5. Comparison of Atomic Distances (Å) and Angles (deg)

compound	Fe−C	Fe−Cp	stagger angle	tilt angle	T_c (K)[a]
1[b]	2.060(6)	1.68(4)	0.0	0.3(3)	~365
3[c]	2.06(1)	1.676(5)		4.8	275
4[d]	2.06(1)	1.677(9)	1.2	6.6	245
6[e]	2.072(5)	1.674		15.6	<4.2
26b[f]	2.07(1)	1.671(6)	0.4(6)	3.9(5)	295
26c[f]	2.068(4)	1.675(2)	5.9(2)	4.2(2)	265
27a[g]	2.06(1)	1.672(8)	3.6(1)	5.9(7)	125
27b[f]	2.07(2)	1.68(1)	16.5(9)	4(1)	>300
27c[f]	2.06(2)	1.668(8)	3.5(5)	6.6(7)	190

[a] Temperature for the localization−delocalization transition on the Mössbauer technique. [b] From ref 7. [c] From ref 33. [d] From ref 19. [e] From ref 11. [f] This work. [g] From ref 29.

controlling the intramolecular electron transfer is the symmetry of the cation. For an asymmetric biferrocenium cation, the two irons are not in equivalent environments and this asymmetry results in a zero-point energy difference for intramolecular electron transfer. In other words, one vibronic state of the mixed-valence cation is energetically more stable than the other state. This explains why a delocalized electronic structure for an asymmetic biferrocenium cation has not been observed.

Recently, Hendrickson and co-workers have addressed counterion effects on intramolecular electron-transfer rates of biferrocenium salts.[13,14] The size, shape, and charge distribution of anions can ultimately affect the solid-state arrangement adopted by a particular system.

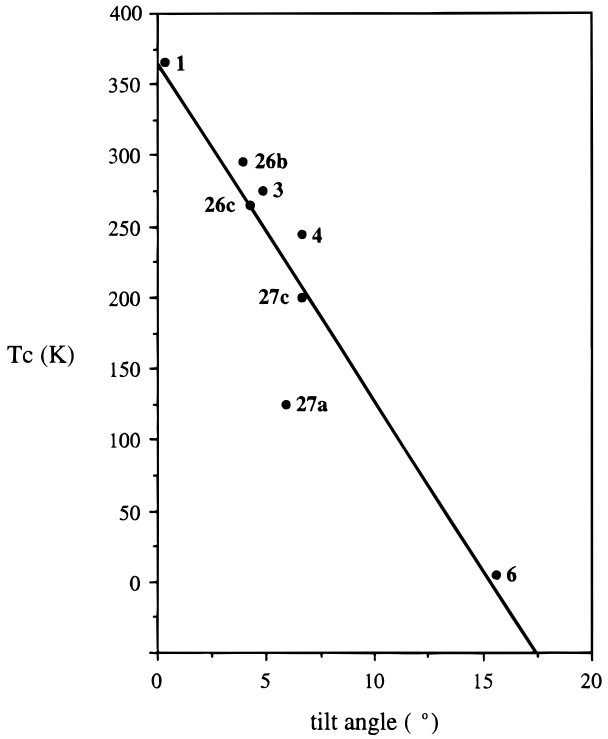

Figure 9. Plot of tilt angle vs transition temperature.

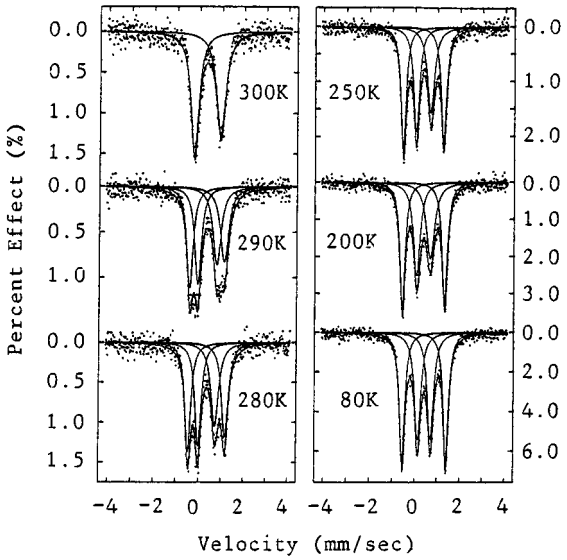

Figure 10. Variable-temperature ^{57}Fe Mössbauer spectra of **26b**.

The interactions between the cation and anion undoubtedly alter the potential energy surface of the mixed-valence molecule and, therefore, the rate of intramolecular electron transfer. Thus, the position of the anion relative to the mixed-valence cation is rather important in determining the rate of electron transfer. In other words, if the charge oscillation of the I_3^- anion is parallel to the electron transfer pathway, this would lead to a stronger ability to pull the charge back and forth in the mixed-valence biferrocenium cation. In this paper, we would like to suggest another factor which also plays an important role in controlling the electron-transfer rate. We have prepared a series of polyalkylbiferrocenium complexes to study the influence of ring tilt between two least-squares-fitted Cp rings on electron

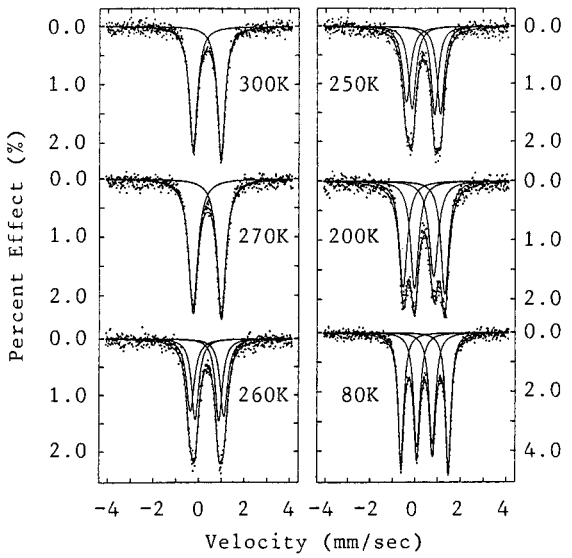

Figure 11. Variable-temperature ^{57}Fe Mössbauer spectra of **26c**.

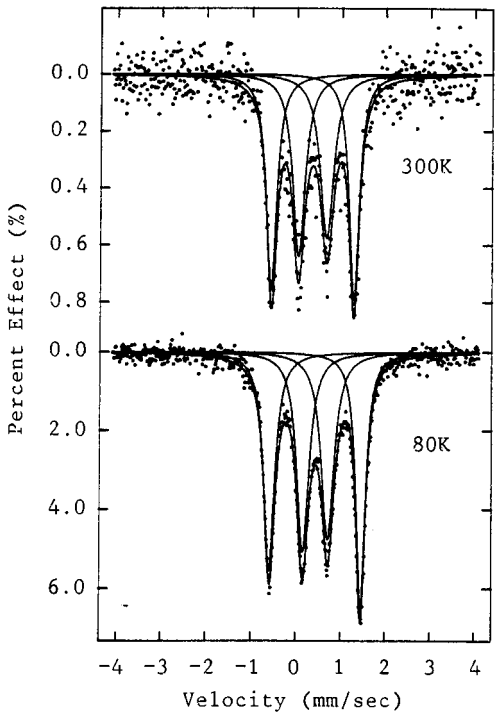

Figure 12. Variable-temperature ^{57}Fe Mössbauer spectra of **27b**.

transfer and to energetically control the electron-transfer rate.

The mixed-valence compounds **26a**−**c** and **27a**−**c** serve as a very sensitive probe of the microscopic structure. We believe that the relatively minor perturbations of the tilt of the Cp ring can have a pronounced effect on the electronic structure and, therefore, the rate of intramolecular electron transfer. As mentioned in the section on the ^{57}Fe Mössbauer studies, the electronic effect of the substituents on the electron-transfer rate was excluded. Here, we suggest that the difference in the rates of electron transfer of **26a**−**c** and **27a**−**c** is a result of the difference in the degree of tilting of the Cp rings from a parallel geometry. As mentioned above, the interactions between the cation and anion play an important role in controlling the magnitude of the

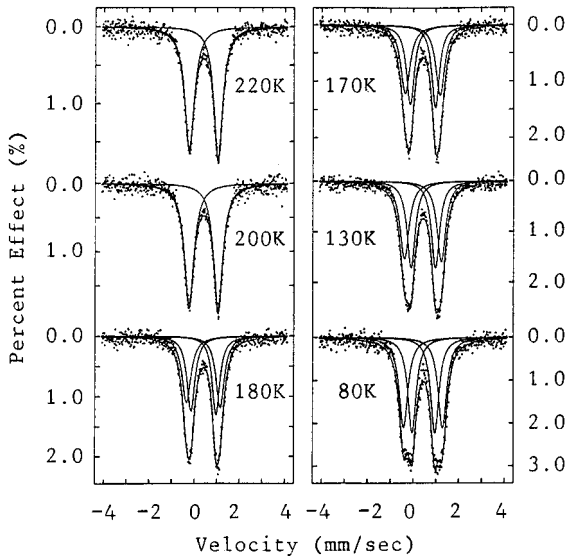

Figure 13. Variable-temperature ^{57}Fe Mössbauer spectra of **27c**.

Table 6. Cyclic Voltammetry for Various Biferrocenes

compound	$E_{1/2}$,[a] V	$\Delta E_{1/2}$,[b] V	Δ,[c] mV	I_c/I_a[d]	K ($\times 10^{-6}$)
ferrocene	0.37		70	0.97	
24a[e]	0.16	0.37	70	1.13	1.87
	0.53		71	1.01	
24b	0.13	0.38	70	0.93	2.76
	0.51		66	1.08	
24c	0.23	0.36	68	0.93	1.26
	0.59		72	1.06	
25a[e]	0.15	0.37	67	0.97	1.87
	0.52		65	1.02	
25b	0.14	0.38	65	0.94	2.76
	0.52		72	1.10	
25c	0.25	0.36	89	0.90	1.26
	0.61		74	1.09	

[a] All half-wave potentials are referenced to the Ag^+/Ag electrode. [b] Peak separation between waves. [c] Peak-to-peak separation between the resolved reduction and oxidation wave maxima. [d] Peak current ratio between the cathode and anode. [e] From ref 29.

electron-transfer rate.[21] Therefore, we only made a comparison for mixed-valence compounds **1**, **3**−**4**, **6**, **26b**,**c**, **27a**,**c** in which the position of the triiodide anion relative to the fulvalenide ligand is perpendicular, rather than parallel to the fulvalenide ligand as found in **9** and **11**. Mixed-valence compounds **10**−**14** are also excluded from the comparison because of the strong van der Waals interaction between the halide substituent in the benzyl unit and the triiodide anion.[21] Under this condition, i.e., same type of stereopacking arrangement, there is a correlation between the tilt angle and the rate of electron transfer in the series of biferrocenium salts (Figure 9). The substituents in the series of biferrocenium cations modify the local structure of the ferrocenyl moiety. In the qualitative view, we suggest that there is an increased ($d_{x^2-y^2}$, d_{xy})-ring overlap as the tilt angle increases.

The electronic ground state of ferrocene is a singlet, $^1A_{1g}$ ($e_{2g}^4a_{1g}^2$), where the one-electron molecular orbitals are predominantly d orbital in character: a_{1g} (d_{z^2}) and e_{2g} ($d_{x^2-y^2}$, d_{xy}).[36] As indicated by magnetic susceptibil-

(36) Duggan, D. M.; Hendrickson, D. N. *Inorg. Chem.* **1975**, *14*, 955.

Table 7. ^{57}Fe Mössbauer Least-Squares-Fitting Parameters

compound	T, K	ΔE_Q[a]	δ[b]	Γ[c]
26b	300	1.158	0.445	0.504, 0.426
	290	1.521	0.454	0.454, 0.338
		0.850	0.462	0.439, 0.351
	280	1.624	0.462	0.366, 0.314
		0.747	0.455	0.413, 0.332
	250	1.782	0.471	0.293, 0.275
		0.647	0.467	0.389, 0.318
	200	1.881	0.488	0.286, 0.272
		0.599	0.488	0.446, 0.364
	80	1.938	0.526	0.284, 0.283
		0.528	0.525	0.343, 0.341
26c	300	1.224	0.452	0.395, 0.419
	270	1.237	0.465	0.457, 0.478
	260	1.474	0.472	0.393, 0.421
		1.024	0.468	0.372, 0.377
	250	1.524	0.473	0.378, 0.438
		0.990	0.472	0.375, 0.400
	200	1.828	0.493	0.403, 0.430
		0.856	0.499	0.476, 0.425
	80	2.086	0.527	0.287, 0.299
		0.690	0.524	0.347, 0.336
27b	300	1.832	0.455	0.267, 0.280
		0.627	0.450	0.368, 0.332
	80	2.029	0.528	0.252, 0.297
		0.554	0.529	0.346, 0.325
27c	300	1.233	0.450	0.433, 0.446
	220	1.280	0.496	0.470, 0.506
	200	1.290	0.501	0.492, 0.515
	180	1.491	0.501	0.446, 0.480
		1.101	0.503	0.407, 0.426
	150	1.583	0.509	0.466, 0.478
		1.068	0.524	0.412, 0.420
	80	1.708	0.525	0.461, 0.465
		0.990	0.540	0.438, 0.441

[a] Quadrupole splitting in mm s^{-1}. [b] Isomer shift referenced to iron-foil in mm s^{-1}. [c] Full width at half-height taken from the least-squares-fitting program. The width for the line at more positive velocity is listed first for each doublet.

Table 8. Absorption Maxima of IT Band and Activation Parameters

compound	ν_{max}[a]	ϵ_{max}[b]	$\Delta\nu_{1/2}$[a] (obsd)	$\Delta\nu_{1/2}$[a] (calcd)	α^2	H_{ab}[a]	K_{et} (10^{-12})
26b	4651	1323	3044	3278	0.0141	552	2.46
26c	4651	1200	3128	3278	0.0132	534	2.30
27b	4651	1388	3128	3278	0.0152	573	2.65
27c	4651	1139	2976	3278	0.0119	507	2.08

[a] In cm^{-1}. [b] Extinction coefficient in M^{-1} cm^{-1}.

ity[37] and EPR measurements,[38] the electronic ground state of ferrocenium is a doublet, $^2E_{2g}$ ($a_{1g}^2e_{2g}^3$). Lauher and Hoffmann have derived the fragment orbitals for a bent $(Cp)_2Fe$ unit from the parallel geometry.[39] The a_{1g} orbital rises rapidly in energy as the Cp rings are bent back. The e_{2g} set also splits into orbitals of a_1 ($d_{x^2-y^2}$) and b_2 (d_{xy}) symmetry. In our previous paper,[29] we performed extended Hückel calculations on a mixed-valence biferrocenium cation with tilt angles varying from 0° to 60° to see how the LUMO−HOMO gap ($E_{e_{1g}} - E_{a_{1g}}$) correlated with the tilt angle. We found the LUMO−HOMO gap decreases as the tilt angle increases. The LUMO molecular level e_{1g} mainly consists of metal antibonding d_{xz} and d_{yz} character. The HOMO level, a_{1g}, is chiefly a d_{z^2} nonbonding orbital. In previous

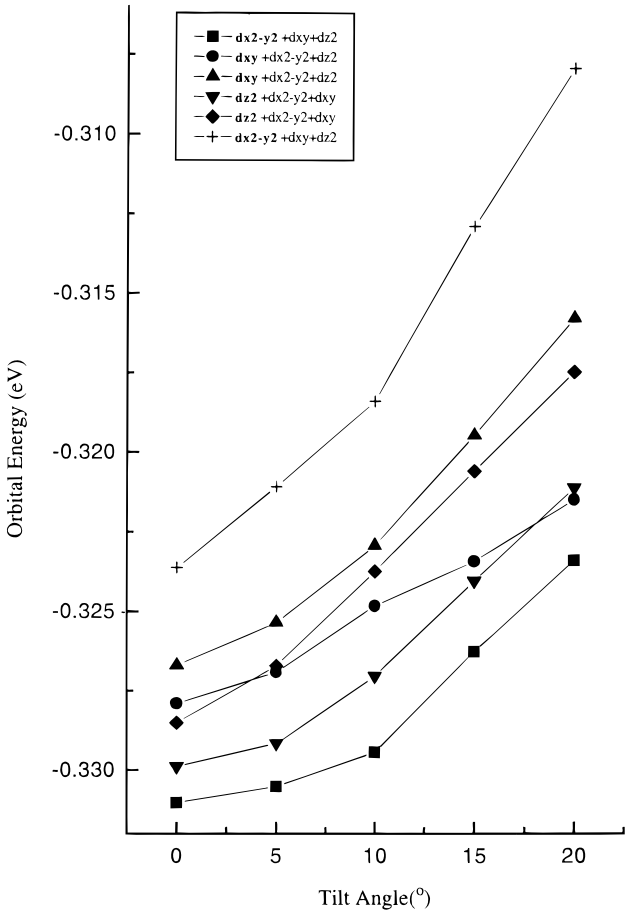

Figure 14. Fragment orbitals for bending biferrocenium triiodide from parallel geometry.

Hückel MO calculations, the e_{2g} ($d_{x^2-y^2}$, d_{xy}) level lies below the a_{1g} (d_{z^2}) level in the mixed-valence biferrocenium cation. However, it is now generally accepted that in mixed-valence biferrocenium cations the e_{2g} level lies above the a_{1g} level, assigned on the basis of the magnetic susceptibility and EPR results.[7,40] For example, the 4.2 K EPR spectrum of biferrocenium triiodide clearly demonstrates the large anisotropy in g values ($g = 3.58$ and 1.72).[7] This large anisotropy and the fast relaxation in the cation clearly demonstrate that the e_{2g} level must lie above the a_{1g} level.

In this paper, density functional theory (DFT) calculations of the energy levels of mixed-valence biferrocenium triiodide with tilt angles varying from 0° to 20° have led to the different highest filled level in this compound. The HOMO molecular level is predominantly metal $d_{x^2-y^2}$ in character. Some metal d_{xy} and d_{z^2} orbitals are also mixed into $d_{x^2-y^2}$. In this case, the metal d_{z^2} level lies below the $d_{x^2-y^2}$ level. Figure 14 illustrates the fragment orbitals for the bending of biferrocenium triiodide from a parallel geometry. As can be seen in Figure 14, the $d_{x^2-y^2}$ and d_{xy} orbitals rise rapidly in energy as the Cp rings are bent back. As shown in Figure 15, the LUMO−HOMO gap decreases as the tilt angle increases. In other words, the metal nonbonding orbitals ($d_{x^2-y^2}$, d_{xy}) start to interact with the ligand pπ orbitals. Hence, bending back the Cp rings leads to a larger extent of metal−ligand interac-

(37) Hendrickson, D. N.; Sohn, Y. S.; Gray, H. B. *Inorg. Chem.* **1971**, *10*, 1559.
(38) (a) Horsfield, A.; Wassermann, A. *J. Chem. Soc. A* **1970**, *3202*. Horsfield, A.; Wassermann, A. *J. Chem. Soc., Dalton Trans.* **1972**, 187. (b) Prins, R.; Kortbeek, A. *J. Organomet. Chem.* **1971**, *33*, C33.
(39) Lauher, J. W.; Hoffmann, R. *J. Am. Chem. Soc.* **1976**, *98*, 1729.
(40) Cowan, D. O.; Collins, R. L.; Kaufman, F. *J. Phys. Chem.* **1971**, *75*, 2025.

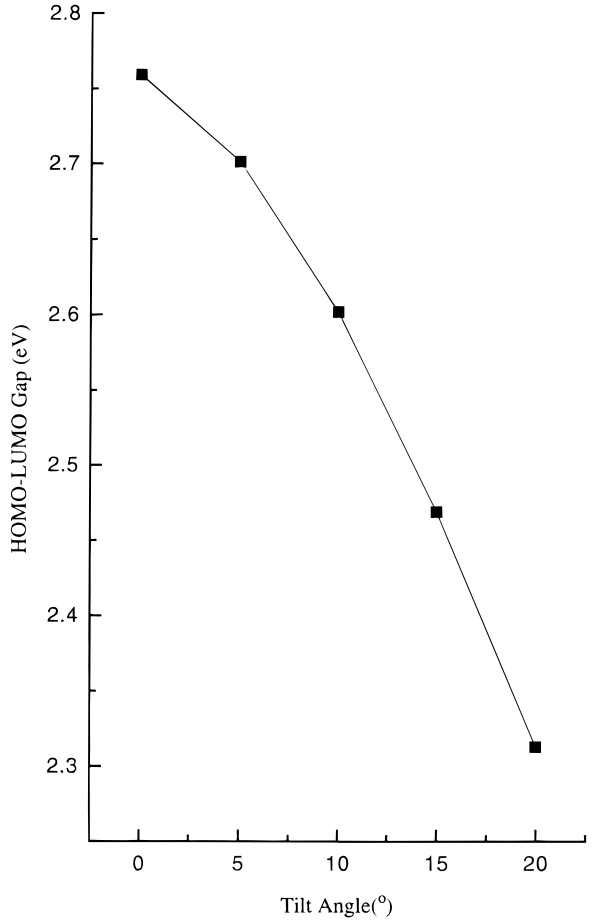

Figure 15. HOMO−LUMO gap as function of tilt angle.

tions, which render intramolecular electron transfer much more facile.

Experimental Section

General Information. All manipulations involving air-sensitive materials were carried out by using standard Schlenk techniques under an atmosphere of N_2. Chromatography was performed on neutral alumina (Merck, activity II). Solvents were dried as follows: benzene, hexane, and ether were distilled from Na/benzophenone; CH_2Cl_2 was distilled from P_2O_5. Samples of 1-propyl-1′-bromoferrocene[8] and 1-benzyl-1′-bromoferrocene[41] were prepared according to the literature procedure.

Propionation of 1-Propyl-1′-bromoferrocene. The propionating reagent was made-up according to the Friedel−Crafts synthesis by mixing 2.2 mL (25 mmol) of propionyl chloride and excess $AlCl_3$ in dry CH_2Cl_2 (50 mL) at 0 °C under N_2. The excess of $AlCl_3$ was filtered off with glass wool.

The propionating reagent was added by means of a dropping funnel over a period of about 1 h to a solution of 1-propyl-1′-bromoferrocene (5.22 g, 17 mmol) in dry CH_2Cl_2 (130 mL) at 0 °C. The reaction mixture was stirred for 6 h and then poured into an ice−water mixture. The resulting mixture was separated after the reduction of the ferrocenium cation with aqueous $Na_2S_2O_3$. The organic layer was washed with saturated aqueous $NaHCO_3$ and H_2O, and then it was dried over $MgSO_4$. The solvent was removed under reduced pressure. The red oily residue was chromatographed on alumina. The second band eluted with *n*-hexane/ethyl acetate (20:1) was **20b** (9% yield). The third band was a mixture of an unknown product and **21b**. This mixture could be separated by rechromatographing on silica gel (70−230 mesh), using *n*-hexane/ethyl acetate (20:1) as the eluent. The first band was unknown, and the second band was **21b** (27.54% yield). The properties of **20b** are as follows. ^{1}H NMR ($CDCl_3$, ppm): 0.96 (t, 3H, -CH_3), 1.18 (t, 3H, -CH_3), 1.48 (m, 1H, −CH_2−), 1.59 (m, 1H, −CH_2−), 2.47 (m, 1H, −CH_2−), 2.66 (m, 1H, −CH_2−), 2.93 (m, 2H, −$COCH_2$−), 4.04 (t, 2H, Cp), 4.31 (t, 2H, Cp), 4.39 (d, 2H, Cp), 4.62 (t, 1H, Cp). MS: M^+ at *m*/*z* 362, 364. The properties of **21b** are as follows. ^{1}H NMR ($CDCl_3$, ppm): 0.96 (t, 3H, −CH_3), 1.19 (t, 3H, −CH_3), 1.56 (m, 2H, −CH_2−), 2.37 (m, 2H, −CH_2−), 2.74 (q, 2H, −$COCH_2$−), 4.07 (t, 2H, Cp), 4.29 (t, 2H, Cp), 4.38 (t, 1H, Cp), 4.67 (s, 1H, Cp), 4.73 (d, 1H, Cp). MS: M^+ at *m*/*z* 362, 364.

Reduction of 20b and 21b. The reduction reaction was carried out by carefully adding, with stirring, a small portion of $AlCl_3$ to a mixture of the corresponding ferrocene compound and $LiAlH_4$ in dry ether. After 30 min, the solution became yellow, an excess of H_2O was added to it, and the ether layer was separated. The ether layer was washed with H_2O and dried over $MgSO_4$. After evaporation of the solvent, the crude product was chromatographed on Al_2O_3, eluting with hexane. The first band was the desired compound. The yields of **22b** and **23b** were approximately 95% and 67%, respectively. The physical properties of **22b** are as follows. ^{1}H NMR ($CDCl_3$, ppm): 0.96 (t, 6H, −CH_3), 1.49 (m, 4H, −CH_2−), 2.29 (t, 4H, −CH_2−), 3.95 (t, 2H, Cp), 4.02 (s, 3H, Cp), 4.17 (t, 2H, Cp). MS: M^+ at *m*/*z* 348, 350. The physical properties of **23b** are as follows. ^{1}H NMR ($CDCl_3$, ppm): 0.93 (t, 6H, −CH_3), 1.51 (m, 4H, −CH_2−), 2.28 (t, 4H, −CH_2−), 3.96 (t, 5H, Cp), 4.18 (t, 2H, Cp). MS: M^+ at *m*/*z* 348, 350.

Benzoylation of 1-Benzyl-1′-bromoferrocene. The benzoylation of **19c** was carried out according the same procedure as the propionation of 1-propyl-1′-bromoferrocene. The red oily residue was chromatographed on alumina. The first band that eluted with *n*-hexane was the starting material. The second band that eluted with *n*-hexane/ethyl acetate (20:1) was **20c** (13% yield), and the third band was **21c** (15% yield). The physical properties of **20c** are as follows. ^{1}H NMR ($CDCl_3$, ppm): 4.00 (d, 1H, −CH_2−), 4.10 (t, 2H, Cp), 4.36 (t, 2H, Cp), 4.42 (t, 1H, Cp), 4.46 (t, 1H, Cp), 4.54 (d, 1H, −CH_2−), 4.54 (m, 1H, Cp), 7.16 (d, 2H, −ph), 7.25 (m, 3H, −ph), 7.43 (t, 2H, −ph), 7.53 (t, 1H, −ph), 7.79 (dd, 2H, −ph). MS: M^+ at *m*/*z* 458, 460. The physical properties of **21c** are as follows. ^{1}H NMR ($CDCl_3$, ppm): 3.79 (s, 2H, −CH_2−), 4.10 (t, 2H, Cp), 4.34 (t, 2H, Cp), 4.50 (t, 1H, Cp), 4.88 (dt, 2H, Cp), 7.27 (m, 5H, −ph), 7.46 (t, 2H, −ph), 7.55 (t, 1H, −ph), 7.86 (d, 2H, −ph). MS: M^+ at *m*/*z* 458, 460. Mp: 81−82 °C.

Reduction of 20c and 21c. The reduction reactions of **20c** and **21c** were carried out according to the same procedure as the reduction of **20b** and **21b**. The physical properties of **22c** are as follows. ^{1}H NMR ($CDCl_3$, ppm): 3.74 (dd, 4H, −CH_2−), 4.00 (t, 2H, Cp), 4.07 (s, 3H, Cp), 4.26 (t, 2H, Cp),7.04 (m, 4H, −ph), 7.15 (m, 6H, −ph). MS: M^+ at *m*/*z* 444, 446. The physical properties of **23c** are as follows. ^{1}H NMR ($CDCl_3$, ppm): 3.67 (s, 4H, −CH_2−), 3.97 (t, 2H, Cp), 4.05 (s, 3H, Cp), 4.25 (t, 2H, Cp), 7.18−7.29 (m, 10H, −ph). MS: M^+ at *m*/*z* 444, 446.

Ullman Coupling Reaction of 22b,c and 23b,c. A mixture of the corresponding bromoferrocene (1 g) and activated Cu (5 g) was heated under N_2 at ∼120 °C for 24 h. After the reaction mixture was cooled to room temperature, it was repeatedly extracted with CH_2Cl_2 until the CH_2Cl_2 extracts appeared colorless. The solvent was evaporated and chromatographed. Compounds **24b**,**c** and **25b**,**c** were recrystallized from hexane. The yields were approximately 90%. The physical properties of **24b** are as follows. ^{1}H NMR ($CDCl_3$, ppm): 0.87 (t, 12H, −CH_3), 1.36 (m, 8H, −CH_2−), 2.03 (m, 8H, −CH_2−), 3.83 (d, 2H, Cp), 3.88 (d, 4H, Cp), 4.12 (d, 4H, Cp), 4.16 (d, 4H, Cp). MS: M^+ at *m*/*z* 538. Mp: 77.2−78 °C. The physical properties of **24c** are as follows. ^{1}H NMR ($CDCl_3$, ppm): 3.46 (s, 8H, −CH_2−), 3.89 (s, 6H, Cp), 4.18 (s, 4H, Cp), 4.26 (s, 4H, Cp), 6.92 (d, 8H, −ph), 7.10 (m, 12H, −ph). MS:

(41) Yamakawa, K.; Hisatome, M.; Sako, Y.; Ichida, S. *J. Organomet. Chem.* **1975**, *93*, 219.

M^+ at m/z 731. Mp: 180.1−180.2 °C. The physical properties of **25b** are as follows. ^{1}H NMR ($CDCl_3$, ppm): 0.86 (t, 12H, $-CH_3$), 1.40 (m, 8H, $-CH_2-$), 2.04 (t, 8H, $-CH_2-$), 3.83 (s, 6H, Cp), 4.14 (t, 4H, Cp), 4.24 (t, 4H, Cp). MS: M^+ at m/z 538. Mp: 51.5−52.5 °C. The physical properties of **25c** are as follows. ^{1}H NMR ($CDCl_3$, ppm): 3.40 (s, 8H, $-CH_2-$), 3.86 (s, 6H, Cp), 4.12 (s, 4H, Cp), 4.24 (s, 4H, Cp), 7.09 (d, 8H, −ph), 7.15 (d, 4H, −ph), 7.22 (d, 8H, −ph). MS: M^+ at m/z 731. Mp: 152−153 °C.

Mixed-Valence Compounds 26b,c and 27b,c. Samples of these mixed-valence compounds were prepared by adding a benzene/hexane (1:1) solution containing a stoichiometric amount of iodine to a benzene/hexane (1:1) solution of the corresponding biferrocene at 0 °C. The resulting dark green crystals were filtered and washed repeatedly with cold hexane. A more crystalline sample can be prepared by slowly diffusing hexane into a CH_2Cl_2 solution containing the corresponding biferrocenium triiodide salt. Anal. Calcd for **26b** ($C_{32}H_{42}Fe_2I_3$): C, 41.82; H, 4.61. Found: C, 41.28; H, 4.56. Anal. Calcd for **26c** ($C_{48}H_{42}Fe_2I_3$): C, 51.88; H, 3.81. Found: C, 51.25; H, 3.82. Anal. Calcd for **27b** ($C_{32}H_{42}Fe_2I_3$): C, 41.82; H, 4.61. Found: C, 41.16; H, 4.50. Anal. Calcd for **27c** ($C_{48}H_{42}Fe_2I_3$): C, 51.88; H, 3.81. Found: C, 51.59; H, 3.86.

Physical Methods. ^{57}Fe Mössbauer measurements were made on a constant-velocity instrument which has been previously described.[21] The absolute temperature accuracy is estimated to be ±5 K, while the relative precision is ±0.5 K. Computer fitting of the ^{57}Fe Mössbauer data to Lorentzian lines was carried out with a modified version of a previously reported program.[42] Velocity calibrations were made using a 99.99% pure 10 μm iron foil. Typical line widths for all three pairs of iron foil lines fell in the range 0.24−0.27 mm s^{-1}. Isomer shifts are reported relative to iron foil at 300 K but are uncorrected for temperature-dependent, second-order Doppler effects. It should be noted that the isomer shifts illustrated in the figures are plotted as experimentally obtained. Tabulated data is provided.

^{1}H NMR spectra were run on a Varian VXR-300 spectrometer. Mass spectra were obtained with a VG-BLOTECH-QUATTRO 5022 system. The near-IR spectra were recorded from 2500 to 900 nm in CH_2Cl_2 by using 1.0 cm quartz cells with a Hitachi U-3501 spectrophotometer.

Electrochemical measurements were carried out with a BAS 100W system. Cyclic voltammetry was perform with a stationary glassy carbon working electrode, which was cleaned after each run. These experiments were carried out with a 1 × 10^{-3} M solution of biferrocene in dry CH_2Cl_2/CH_3CN (1:1) containing 0.1 M of (n-C_4H_9)$_4$NPF$_6$ as the supporting electrolyte. The potentials quoted in this work are relative to a Ag/AgCl electrode at 25 °C. Under these conditions, ferrocene shows a reversible one-electron oxidation wave ($E_{1/2}$ = 0.37 V).

The single-crystal X-ray determinations of compounds **24b**,**c**, **25b**,**c**, **26b**,**c**, and **27b**,**c** were carried out on an Enraf-Nonius CAD4 diffractometer at 298 K. Absorption corrections were made with empirical ψ rotation. The X-ray crystal data are summarized in Tables 1 and 2. Selected bond distances and angles are given in Tables 3 and 4. Tables of the final positional parameters for all atoms, complete bond distances and angles, and thermal parameters of these compounds are given in the Supporting Information.

Structure Determination of 24b. An orange crystal (0.1 × 0.1 × 0.15 mm), which was grown by slow evaporation from a hexane solution, was used for data collection at 298 K. Cell dimensions were obtained from 20 reflections with 11.82° < 2θ < 30.10°. The $\theta-2\theta$ scan technique was used to record the intensities for all reflections for which 1° < 2θ < 44.9°. Of the 1791 unique reflections, there were 1321 reflections with $F_o > 2.0\sigma F_o^2$, where σF_o^2 was estimated from counting statistics. Absorption corrections were applied. These data were used in the final refinement of the structural parameters.

A three-dimensional Patterson synthesis was used to determine the heavy-atom positions, which phased the data sufficiently well to permit location of the remaining non-hydrogen atoms from Fourier synthesis. All non-hydrogen atoms were refined anisotropically. Hydrogen atoms were calculated at ideal distances.

Structure Determination of 24c. An orange crystal (0.5 × 0.5 × 0.3 mm) was obtained following the same procedure as described for **24b**. Data were collected to a 2θ value of 50.0°. Absorption corrections were also made. The unit-cell dimensions were obtained from 20 reflections with 9.3° < 2θ < 14.3°. Of the 3270 unique reflections, there were 2211 with $F_o > 3.0\sigma F_o^2$. These data were used in the final refinement of the structural parameters. The structure was solved and refined as described for **24b**.

Structure Determination of 25b. An orange crystal (0.10 × 0.15 × 0.25 mm) was obtained following the same procedure as described for **24b**. The unit-cell dimensions were obtained from 25 reflections with 19.72° < 2θ < 26.60°. Of the 1765 unique reflections, there were 1546 with $F_o > 2.0\sigma F_o^2$. These data were used in the final refinement of the structural parameters. The structure was solved and refined as described for **24b**.

Structure Determination of 25c. An orange crystal (0.08 × 0.07 × 0.15 mm) was obtained following the same procedure as described for **24b**. The unit-cell dimensions were obtained from 25 reflections with 13.60° < 2θ < 25.90°. Of the 2294 unique reflections, there were 1118 with $F_o > 2.0\sigma F_o^2$. These data were used in the final refinement of the structural parameters. The structure was solved and refined as described for **24b**.

Structure Determination of 26b. A dark black crystal (0.10 × 0.15 × 0.25 mm) was obtained when a layer of hexane was allowed to slowly diffuse into a CH_2Cl_2 solution of **26b**. Data were collected to a 2θ value of 44.9°. The cell dimensions were obtained from 25 reflections with 2θ in the range 19.72−26.60°. The data were also corrected for absorption with an empirical ψ rotation. Of the 2227 unique reflections, there were 1423 with $F_o^2 > 2.0\sigma F_o^2$. These data were used in the final refinement of the structural parameters. Structure refinement was carried out in the same manner as described for **24b**. The greatest residual electron density upon completion of refinement was in the vicinity of the iodide atoms.

Close examination of difference Fourier maps in the final stage of the structure solution revealed one disordered propyl group in each Cp ring, labeled C15−C16 and C15′−C16′. The site occupancy factor of the propyl substitutent was set equal to 0.5.

Structure Determination of 26c. A dark black crystal (0.20 × 0.20 × 0.25 mm) was obtained following the same procedure as described for **26b**. Data were collected to a 2θ value of 45.0°. The cell dimensions were obtained from 25 reflections with 2θ in the range 22.68−28.22°. Of the 2730 unique reflections, there were 2273 with $F_o^2 > 2.0\sigma F_o^2$. Structure refinement was carried out in the same manner as described for **24b**.

The final structure solution revealed a badly disordered triiodide ion. Iodine atom labeled I2 was refined with two positions, each at 50% occupancy. Iodine atom labeled I1 was refined with three positions, each at 33% occupancy.

Structure Determination of 27b. A dark black crystal (0.08 × 0.08 × 0.15 mm) was obtained following the same procedure as described for **26b**. Data were collected to a 2θ value of 45.0°. The cell dimensions were obtained from 25 reflections with 2θ in the range 12.48−24.50°. The data were also corrected for absorption. Of the 2254 unique reflections, there were 1329 with $F_o^2 > 2.0\sigma F_o^2$. Structure refinement was carried out in the same manner as described for **24b**.

Structure Determination of 27c. A dark black crystal (0.05 × 0.10 × 0.10 mm) was obtained following the same

(42) Lee, J. F.; Lee, M. D.; Tseng, P. K. *Chemistry* **1987**, *45*, 50.

procedure as described for **26b**. Data were collected to a 2θ value of 44.9°. The cell dimensions were obtained from 25 reflections with 2θ in the range 13.40−28.38°. The data were also corrected for absorption. Of the 2715 unique reflections, there were 1819 with $F_o^2 > 2.5\sigma F_o^2$. Structure refinement was carried out in the same manner as described for **24b**.

Molecular Orbital Calculations. The molecular structure of biferrocenium triiodide geometry is taken from the X-ray diffraction result. Theoretical calculations of the fragment orbitals for bending of biferrocenium triiodide from a parallel geometry to a structure with a tilt angle of up to 20°. DFT calculations are applied to this compound. The basis set used in DFT is double numerical plus polarization,[43,44] which is comparable to 631G**. The local density approximation is applied in the DFT calculation, where the VWN potential[45] is used. DFT computation is performed on power challenge with the DMOL[44] program.

Acknowledgment. Acknowledgments are made to the National Science Council (Grant No. NSC86-2113-M-110-003), Taiwan, ROC, and Department of Chemistry at Sun Yat-sen University. Thanks are also made to the National High Performance Super Computer Center for the use of their computer and software.

Supporting Information Available: Complete tables of positional parameters, bond lengths and angles, and thermal parameters for **24b**,**c**, **25b**,**c**, **26b**,**c**, and **27b**,**c** (34 pages). Ordering information is given on any current masthead page.

OM961032R

(43) (a) Von Barth, U.; Hedin, L. *J. Phys. C* **1972**, *5*, 1629. (b) Versluis, L.; Zeigler, T. *J. Chem. Phys.* **1988**, *88*, 3322.

(44) (a) Delly, B. *J. Chem. Phys.* **1990**, *92*, 508. DMol is available commerically from BIOSYM Technologies, San Diego, CA. (b) Delly, B. *Density Functional Methods in Chemistrry*; Labanowski, J., Andzelm, J., Eds.; Springer-Verlag: New York, 1991; p 101. (c) Delly, B. *J. Chem. Phys.* **1991**, *94*, 7245.

(45) Vosko, S. J.; Wilk, L.; Nusair, M. *Can. J. Phys.* **1980**, *58*, 1200.